Hindawi
Shock and Vibration
Volume 2021, Article ID 1555295, 12 pages
https://doi.org/10.1155/2021/1555295

Research Article

Research on Impact Stress Transfer Characteristics of Lunar Rock Coring Drill

Peng Li,[1] Yizhuo Wang,[1,2] Bo Xu,[1] Junwei Liu,[3] and Weiwei Zhang[3]

[1]*Mechanical Engineering College, Yanshan University, Qinhuangdao 066004, China*
[2]*Mechanical Engineering College, Beihua University, Jilin 132022, China*
[3]*State Key Laboratory of Robotics and System, Harbin Institute of Technology, Harbin 150001, China*

Correspondence should be addressed to Bo Xu; 474144069@qq.com and Weiwei Zhang; zweier@hit.edu.cn

Received 21 June 2021; Accepted 20 August 2021; Published 15 September 2021

Academic Editor: Bao-Jun Shi

In the whole lunar surface drilling and sampling task, it is critical to make the operation of the drilling and sampling impact system efficient and reliable. This paper focuses on how to improve the impact stress obtained at the cutting edge of the drill bit. Firstly, with the objective of maximizing the output impact energy, the design parameters of the percussive mechanism are optimally selected; based on the one-dimensional stress wave transfer theory, the collision input model and transfer models of impact stress in the drilling tool are established. Secondly, in order to verify the above design parameters and theoretical models, the percussive drive characteristics' test and the transfer characteristics' tests of impact stress in the drill stem and drilling tool joints are carried out in turn. The experimental results are consistent with the theoretical analysis, which clarifies the transfer characteristics of the impact stress at the various stages of generation, incidence, and transfer to the cutting edge. It was finally found that increasing the percussive frequency and impact energy of the percussive mechanism as well as the contact stiffness of the collision surface can increase the incident impact stress of the drilling tool, while reducing the length of the screw connection between the drill bit and the drill stem can reduce the impact stress loss. This provides a theoretical reference for the design of the percussive mechanism and drilling tools in lunar surface drilling and sampling tasks.

1. Introduction

Sampling of lunar regolith samples for return is an important part of lunar exploration missions [1], among which drilling sampling is widely adopted by various countries because of many advantages such as high efficiency, stability, and effective retention of rational information of the lunar regolith layer [2, 3]. Compared with geological drilling, lunar surface drilling and sampling faces the interference of low gravity, high vacuum, and unknown mechanical properties of the lunar regolith, and its drilling efficiency is significantly reduced [4, 5]. In order to improve the drilling crushing efficiency of lunar rock simulants, a certain impact force can be applied during rotary drilling to make it assist in crushing lunar rocks [6, 7]. However, due to the long length of the lunar rock coring auger, there is a large amount of energy loss in the transfer of impact force from the top of the auger to the drill bit, making it difficult to form a visible impact crushing pit on the lunar rock surface. In addition, the drilling tool system can only provide a limited amount of power due to the limitations of rocket carrying capacity and other factors [8, 9]. Therefore, in order to obtain greater energy at the drill bit, it is necessary to study the impact action of coring drilling tools and their transmission characteristics.

At present, the mechanical response characteristics in drilling tools can be explained by the theory of impact stress waves. Among them, Li tested the stress wave curves of impact pistons with different lengths based on the stress wave testing technique and calculated the impact performance to obtain the relationship between impact force and collision coefficient of restitution [10]; Hustrulid and Mate et al. studied the energy transfer efficiency from the perspective of the shape size of the drill stem and drill bit and

the contact conditions between the bit and the rock, respectively [11, 12]; Wang et al. introduced an elastic model of the drilling tool joint and carried out an experimental study [13]; Li and Ma developed a linear contact nonlinear spring-damped contact force model describing rigid body acceleration and stress wave acceleration based on the one-dimensional stress wave transfer theory [14]; Yang et al. conducted a computational analysis of the energy transfer efficiency of four stress waveforms in the drilling tool [15]; Yuan et al. studied the influence law of axial static load on the stress amplitude of the variable cross section [16]. In this paper, we focus on how to improve the impact stress obtained at the cutting edge of the drill bit and carry out experimental research from two perspectives of increasing the stress input and reducing the loss in the transmission process, respectively. Firstly, the design parameters of the percussive mechanism are optimally selected with the objective of maximizing the output impact energy; secondly, the impact stress collision input model and stress transfer model in the drilling tool are established according to the stress wave transfer theory; finally, the above design parameters and the theoretical model are verified experimentally.

2. Stress Transfer Model in the Coring Drilling Tool under Impact Action

The transmission path of impact stress in the drilling tool during the lunar rock drilling and sampling is shown in Figure 1, in which the percussive drive mechanism in the drilling mechanism provides kinetic energy to the percussive hammer and generates a single impact energy; the impact force is generated by the percussive hammer after collision with the anvil and is sequentially transferred to the lunar rock through the anvil, drill stem, drill bit, and finally by the cutting edge. Table 1 shows the relevant parameters in the impact stress transfer process.

2.1. Parameter Optimization of the Percussive Mechanism. The percussive drive mechanism is loaded by intermittent cams to drive the spring mass block to achieve reciprocating motion. Therefore, with certain drive power consumption, the output impact energy can be increased by a reasonable design of the percussive mechanism [17, 18].

Figure 2 shows the three-dimensional model of the percussive mechanism and the force analysis diagram; then, the percussive mechanism power consumption P_C, cam rotation speed n_C, and cam torque T_C are

$$P_C = \frac{2\pi \cdot n_C \cdot T_C}{60},$$

$$n_C = \frac{60 \cdot f_P}{n_{Cb}},$$

$$T_C = \frac{\left(m_P \cdot g + k_P \cdot s_C + F_{p0} + m_p \cdot s_C\right)}{1 - \left(\tan\,\alpha_C + E_\delta / 1 - E_\delta \cdot \tan\,\alpha_C\right) \cdot \mu_C} \cdot \frac{\tan\,\alpha_C + E_\delta}{1 - E_\delta \cdot \tan\,\alpha_C} \cdot R_C, \tag{1}$$

where f_P is the percussive frequency; n_{Cb} is the number of convex contour line bumps; S_C is the percussive hammer displacement; F_{P0} is the percussive spring preload; E_δ is the percussive hammer roller equivalent rolling friction coefficient; α_C is the pressure angle; μ_C is the sliding friction coefficient; R_C is the cylindrical cam base circle radius; k_P is the percussive spring stiffness coefficient; and m_P is the percussive hammer mass. The percussive spring stiffness coefficient in equation (1) can be obtained by inversely calculating the required impact energy, i.e.,

$$k_P = \frac{2W_P}{\left(h_{p0} + h_C\right)^2 - h_{p0}^2}, \tag{2}$$

where h_{p0} is the percussive spring preload displacement and h_C is the maximum action displacement of the percussive hammer. Among the above parameters, the percussive frequency and single impact energy are the initial optimization indexes of the system, the roller radius and rolling friction coefficient depend mainly on the material of the cam and roller and the contact stiffness, while the percussive spring stiffness and spring preload are related to its initial installation position. Therefore, the variable parameters can be summarized as follows:

$$X_P = \left\{k_p, h_C, h_{P0}, m_p, n_{Cb}, \beta_{C1}, R_C\right\}^T, \tag{3}$$

where β_{C1} is the cylindrical cam thrust motion angle and needs to meet

$$\frac{2h_C}{R_C \cdot \tan\left[\alpha_C\right]} \le \beta_{C1} \le \frac{2\pi}{n_{Cb}} \cdot \left(1 - f_P \cdot \sqrt{\frac{m_P}{k_p}} \cdot a\,\cos\frac{h_{P0}}{h_C + h_{P0}}\right). \tag{4}$$

The remaining parameters of the design variables need to satisfy the constraints of the structural dimensions of the percussive mechanism in addition to the two constraints mentioned above. Therefore, the constraint parameters of the percussive mechanism can be discretized in Table 2, and the parameters can be optimized by the enumeration method.

After arranging and combining the above design parameters, 49104 groups of parameters can be obtained. Then, the minimum power consumption of the percussive mechanism is found, and its corresponding design parameter group is the results of optimal selection, as shown in Table 2.

2.2. Model of Impact Stress Collision Input Drilling Tools. It can be seen from Figure 2 that the impact force is formed on the contact surface between the percussive hammer and the anvil. The collision model can be regarded as a spring damping model, and the equivalent model is shown in Figure 3 [19, 20].

According to the characteristic equation of one-dimensional stress wave transfer, it can be deduced that the impact force generated by the collision of the mass block and the elastic rod should satisfy the following equation:

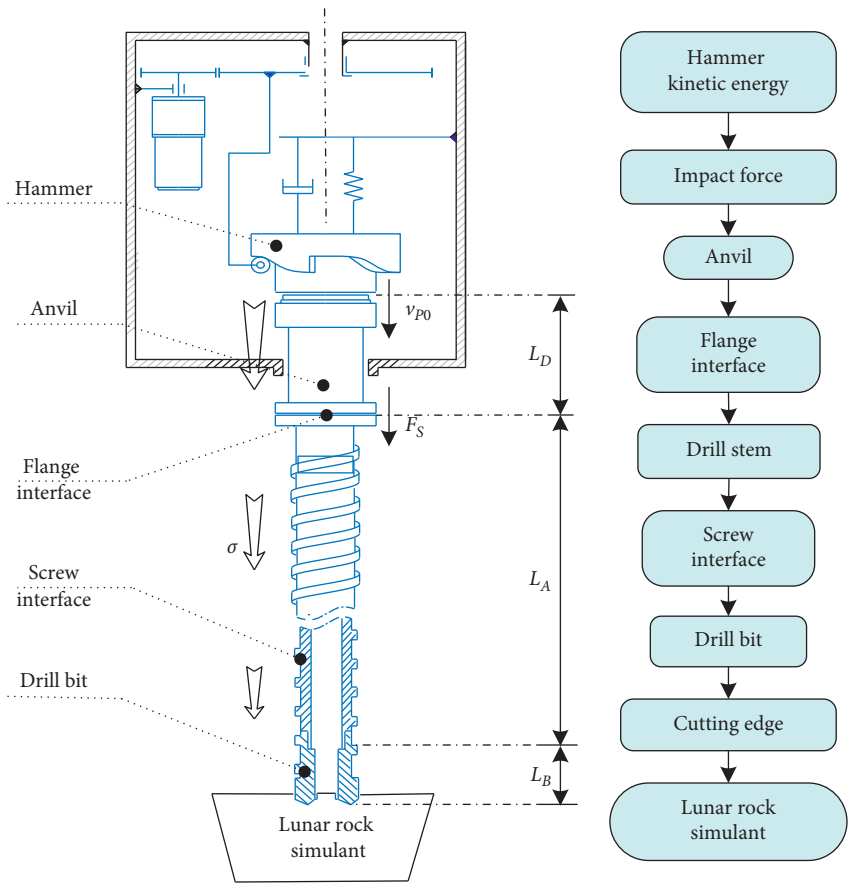

Figure 1: The transmission diagram of impact stress in the lunar rock drilling process.

Table 1: Constant parameters used in the transmission analysis of impact stress on drill.

Parameters	Symbols	Numerical value	Unit
Input impact energy	W_P	0.8~4	J
Percussive frequency	f_P	0~20	Hz
Anvil length	L_D	230	mm
Drill stem length	L_A	2600	mm
Length of the drill bit	L_B	46	mm
Outside diameter of the drill stem	D_{Ao}	31	mm
Drill stem inner diameter	D_{Ai}	25.5	mm
Cross-sectional area of the drill stem	A_D	189	mm^2
Materials		Steel grade 45	
Elastic modulus	E	210×109	$N{\cdot}m^{-1}$
Density	ρ	7850	$kg{\cdot}m^{-3}$

$$m_P\ddot{x}_P = -k_s(x_P - x_D) - c_s(\dot{x}_P - \dot{x}_D),$$
$$c_s\dot{x}_P + k_s x_P = \left(c_s + \frac{EA_D}{C}\right)\dot{x}_D + k_s x_D. \quad (5)$$

From the state of the mass block and elastic rod at the moment before contact ($t = 0$), the initial boundary conditions of the model are determined as follows:

$$x_P = 0,$$
$$\dot{x}_P(0) = v_0, \quad (6)$$
$$x_D = 0,$$

where v_0 is the impact velocity; k_s is the contact stiffness of the percussive hammer-drilling tool collision; c_s is the equivalent damping coefficient of the percussive hammer-

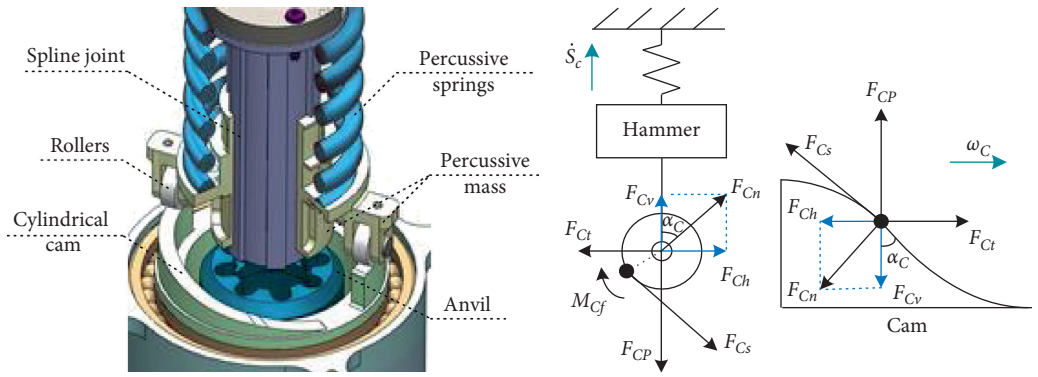

Figure 2: (a) 3D configuration of the percussive mechanism. (b) Force analysis model.

Table 2: The constraint parameters of the percussive mechanism.

Parameter name	Symbols	Value interval	Optimum result
Spring stiffness coefficient	k_P	< 20000	13500 N/m
Hammer amplitude	h_C	5, 6, . . ., 20	8 mm
Spring preload displacement	h_{P0}	5, 6, . . ., 20	20 mm
Hammer mass	m_P	180, 280, . . ., 580	180 g
Number of convex contour line bumps	n_{Cb}	2, 3, 4	2
Cam thrust motion angle	β_{C1}	10, 55, . . ., 180	155°
Cam base circle radius	R_C	25, 26, . . ., 35	33 mm

Optimum indexes: percussive frequency $f_P = 20$ Hz; single impact energy $W_P = 2.6$ J. Constraint parameters: cam speed $n_C < 3000$; roller equivalent rolling friction coefficient $R_{Cf} = 0.0039$; sliding friction coefficient $\mu_C = 0.5$; permissible pressure angle $(\alpha_C) < 20$.

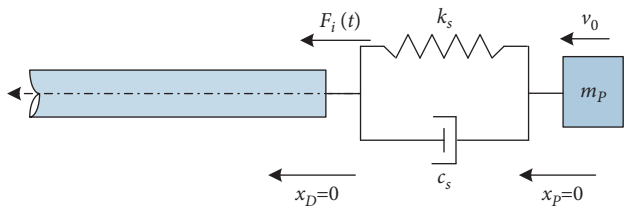

Figure 3: The mechanics simplified model of the hammer impact drill process.

drilling tool collision; x_P is the percussive hammer displacement; x_D is the displacement of the mass point on the contact surface; A_D is the contact area of the percussive hammer-drilling tool collision; E is the elastic modulus of the drill stem; and C is the stress wave propagation velocity. The Laplace transform of equation (5) is

$$\begin{aligned}\left(s^2 + 2\xi s + \omega_0^2\right)x_P^* - \left(2\xi s + \omega_0^2\right)x_D^* &= v_0,\\ \left(2\xi s + \omega_0^2\right)x_P^* - \left[2(\xi + \eta)s + \omega_0^2\right]x_D^* &= 0,\end{aligned} \tag{7}$$

where $x_P^*(s)$ is the Laplace transform of $x_P(t)$ and $x_D^*(s)$ is that of $x_D(t)$. ζ, η, and ω_0 are as follows:

$$\begin{aligned}\xi &= \frac{c_s}{2m_P},\\ \eta &= \frac{EA_D}{2Cm_P},\\ \omega_0^2 &= \frac{k_S}{m_P}.\end{aligned} \tag{8}$$

Then, the inverse Laplace transform of equation (7) can be obtained as follows:

$$x_P(t) = \frac{v_0}{2\eta}\left\{\begin{array}{l} 1 - e^{-\alpha t}\cos\ \omega t \\ +\beta_1 e^{-\alpha t}\sin\ \omega t \end{array}\right\},$$
$$x_D(t) = \frac{v_0}{2\eta}\left\{\begin{array}{l} 1 - e^{-\alpha t}\cos\ \omega t \\ -\beta_1 e^{-\alpha t}\sin\ \omega t \end{array}\right\}, \quad (9)$$

where

$$\alpha = \frac{\omega_0^2 + 4\xi\eta}{4(\xi+\eta)},$$
$$\beta_1 = \frac{8\eta^2 - \omega_0^2 + 4\xi\eta}{4(\xi+\eta)\omega},$$
$$\beta = \frac{\omega_0^2 - 4\xi\eta}{4(\xi+\eta)\omega}, \quad (10)$$
$$\omega^2 = \frac{16\eta^2\omega_0^2 - \left(\omega_0^2 - 4\xi\eta\right)^2}{16(\xi+\eta)^2},$$
$$\varphi = \arcsin\frac{\alpha - \omega\beta}{\sqrt{1+\beta^2}\sqrt{\alpha^2+\omega^2}}.$$

Combining the above equation, the incident impact stress obtained by the drilling tool is

$$\sigma_i(t) = \frac{m_P v_0\sqrt{1+\beta^2}\sqrt{\alpha^2+\omega^2}}{A_D}\cdot e^{-\alpha t}\sin(\omega t + \varphi). \quad (11)$$

The above equation is the attenuation equation of the impact stress at the position coordinate of 0. From equation (11), it can be seen that the impact stress obtained by the drilling tool is a sinusoidal function of time, and its amplitude decay trend is exponential. In addition, by substituting each parameter of Table 2 into the above equation, the trend of impact stress with initial velocity v_0 and contact stiffness k_s can be obtained as shown in Figure 4.

As can be seen from Figure 4, the incident impact stress obtained by the drilling tool increases with the speed of the percussive hammer, and it basically follows a linear trend of increase. In addition, the stress amplitude increases gradually with the increase of contact stiffness of the collision surface, and the time taken to reach the peak becomes smaller.

2.3. Transfer Model of Impact Stress in Drilling Tools

2.3.1. Transfer Model in the Drill Stem. In order to analyze the attenuation characteristics of impact stress along the axial direction of the drilling tool, the following assumptions are made: (I) since the length of the anvil and bit is much smaller than that of the drill stem (the length of the drill stem is 2510 mm, while the length of the drill bit and the anvil is 50 mm and 150 mm, respectively), the stress attenuation in the above two components can be disregarded, and only the attenuation of impact stress in the drill stem is considered; (II) the drill stem is treated as a thin-walled smooth rod, i.e., the cross-sectional area of each section is the same size; (III) the drill stem material is treated as uniform, i.e., the value of impact stress attenuation rate is constant.

An infinitesimal in the drill stem is taken for analysis (as shown in Figure 5), and it can be obtained:

$$\sigma\eta_\sigma \mathrm{d}x = \sigma - (\sigma + d\sigma). \quad (12)$$

The impact stress at the position coordinate $x = 0$ of the drilling stem is set to σ_0. The attenuation equation of the impact stress with displacement is obtained by integrating equation (12) as

$$\sigma = \sigma_0 e^{-\eta_\sigma x}, \quad (13)$$

where η_σ is the impact stress attenuation coefficient in m^{-1}.

2.3.2. Transfer Model at the Drilling Tool Joints. The drilling tool joints mainly include the flange connection interface between the anvil and the drill stem and the screw connection interface between the drill stem and the drill bit. Based on the presence or absence of axial relative motion during the impact process, the stress transfer models at the connection interface are equated to the rigid body mass model and mass damping model, respectively. The equivalent models are shown in Figure 6.

According to the equivalent model, the incident and transmitted stresses at the flange interface and the incident and transmitted stresses at the screw interface can be derived to satisfy the following differential equations, respectively:

$$\frac{M_F}{2Z}\frac{\mathrm{d}\sigma_t}{\mathrm{d}t} + \sigma_t = \sigma_i, \quad (14)$$

$$\frac{M_T}{2Z}\frac{\mathrm{d}\sigma_t}{\mathrm{d}t} + \left(1 + \frac{c_T}{2Z}\right)\sigma_t = \sigma_i, \quad (15)$$

where M_F is the equivalent rigid body mass of the flange interface; Z is the drilling tool wave resistance coefficient; σ_i is the incident stress of the interface; σ_t is the transmitted stress of the interface; M_T is the equivalent mass of the screw interface; and c_T is the equivalent damping of the screw interface.

When solving the transfer efficiency, in order to simplify the calculation model, incident impact stress equation (11) obtained above is simplified to the exponential form shown in the following equation:

$$\sigma_i = \sigma_0 e^{-\left(Z/m_p\right)t}. \quad (16)$$

Then, substituting equation (16) into equations (14) and (15), respectively, the impact stress transfer efficiency at the flange interface and screw interface can be obtained as η_F and η_T, respectively.

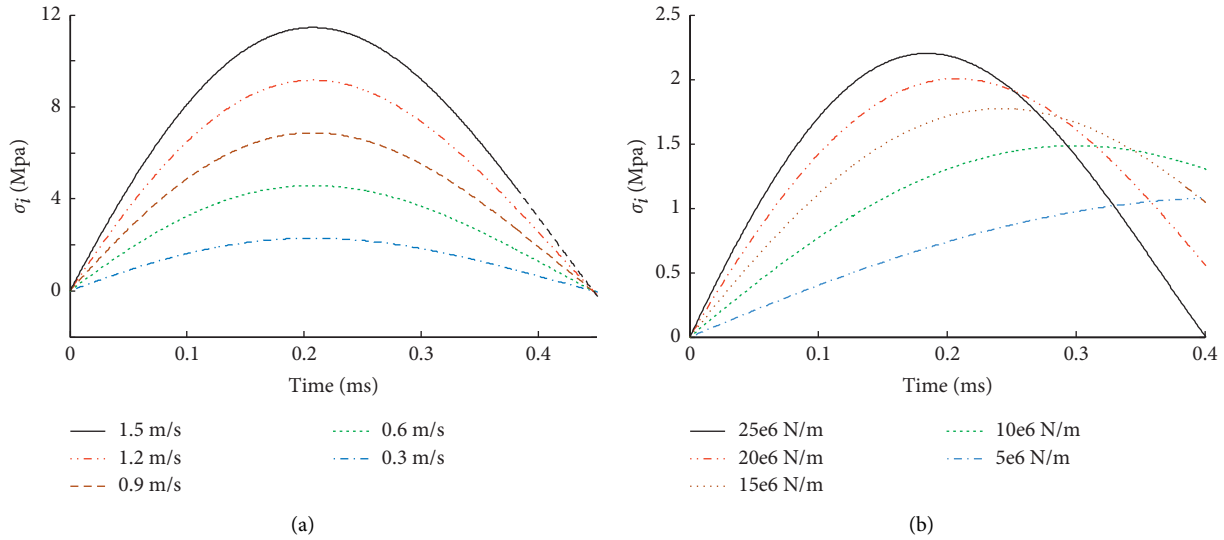

Figure 4: The waveform diagram of incident impact stress. (a) Curves of impact stress vs. impact velocity. (b) Curves of impact stress vs. hammer contact stiffness.

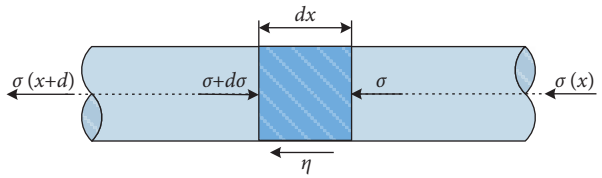

Figure 5: The drilling tool impact stress transmission diagram.

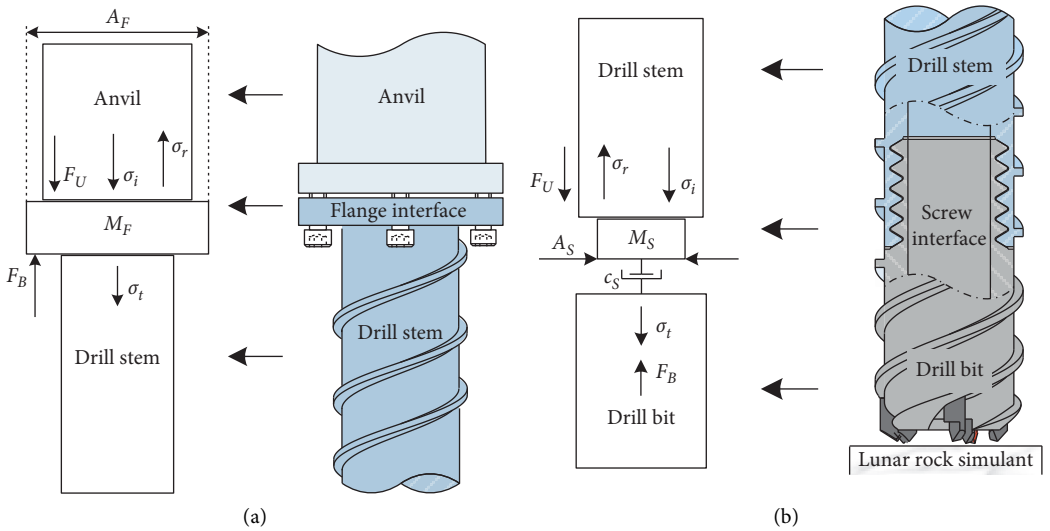

Figure 6: Stress transfer analysis of the flange/screw interface. (a) The rigid body mass model (flange interface). (b) The mass damping model (screw interface).

$$\eta_F = \frac{E_t}{E_i} = \frac{A_F c/E \int_0^\infty \sigma_t^2 \mathrm{d}t}{A_F c/E \int_0^\infty \sigma_i^2 \mathrm{d}t} = \frac{2}{2 + K_{Fmr}}, \tag{17}$$

$$\eta_T = \frac{E_t}{E_i} = \frac{A_T c/E \int_0^\infty \sigma_t^2 \mathrm{d}t}{A_T c/E \int_0^\infty \sigma_i^2 \mathrm{d}t} = \frac{4 + \left(4K_{Tmr}/2 + K_{Tczr}\right) - \left(16K_{Tmr}/K_{Tmr} + K_{Tczr} + 2\right)}{\left(K_{Tczr} - K_{Fmr} + 2\right)^2}, \tag{18}$$

where E_i is the energy of the incident stress wave; E_t is the energy of the transmitted stress wave; $K_{Fmr} = M_F/m_P$; $K_{Tmr} = M_T/m_P$; and $K_{Tczr} = c_T/Z$.

Figure 7(a) shows the curve of stress transfer efficiency η_F versus K_{Fmr}, and Figure 7(b) shows the trend of stress transfer efficiency η_T with K_{Tmr} when changing K_{Tczr}.

3. Experimental Verification

In order to verify the design parameters of the percussive drive mechanism and the above theoretical model, it is necessary to carry out the percussive drive characteristics' test and the transfer characteristics' test of the impact stress in the drill stem and the drilling tool joints, respectively.

3.1. Percussive Drive Characteristics' Experiment. Before conducting the experiment, the single impact energy of the percussive mechanism was first calibrated. The calibration method is to measure the maximum velocity of the percussive hammer before colliding with the drilling tool by using a high-speed camera and then solve for the single impact energy.

After multiple measurements, the maximum velocity is −5.045 m/s, and the single impact energy can be calculated as 2.3 J (less than the design value of 2.6 J) from the following equation:

$$W_P = \frac{1}{2}k_P \cdot \left(h_C + h_{p0}\right)^2 - \frac{1}{2}k_P \cdot h_{P0}^2 = \frac{1}{2}m_P \cdot v_P^2. \tag{19}$$

Then, the percussive mechanism is designed by using the above optimally selected parameters, and the experiment is carried out on the test platform. The velocity curve of the percussive hammer is shown in Figure 8(a).

Figure 8(b) shows the comparison curve between the experimental value of percussive driving power consumption and the theoretical optimization results. It can be seen from the figure that there is little difference between the theoretical value and the experimental value of the maximum driving power consumption, which are 141.8 W and 148.2 W, respectively, and the variation tendency of the two is basically the same. Therefore, the design parameters of the percussive mechanism optimally selected by the above method can meet the requirements of the drilling tool for the percussive frequency and impact energy in the sampling process.

3.2. Transfer Characteristics' Experiment in the Drill Stem. Figure 9 shows the drilling tool impact stress transfer characteristics' test system. During the impact process, the penetration mechanism can apply a certain static pressure to the drilling tool, thus ensuring that the drilling tool is always in contact with the lunar rock simulant. Fiber optic grating sensors are attached to the drilling tool surface along the axial direction to measure the stress and strain at different locations of the drilling tool after the impact action.

According to the previous simulation analysis experience of the impact stress transfer characteristics, the fiber grating sensor is pasted near the lower surface of the spiral wing [21], and four installation measuring points are necessary, while they should be installed at an interval of 800 mm. The relative position between the measuring point and the drilling tool is shown in Figure 10. In addition, in order to reduce the influence of temperature error, the fiber grating sensor at each measuring point is encapsulated with strong adhesive [22].

Firstly, the attenuation law of impact stress in the drill stem is studied. Taking the percussive frequency of 2 Hz and the single impact energy of 1.25 J as the impact input parameters and setting the static pressure between the drilling tool and the lunar rock simulant as 0 N, the variation trend of impact stress with time at different positions can be obtained, as shown in Figure 11.

From Figure 11, it can be seen that the impact stress reaches its maximum value successively during the transmission from measuring point 1 to measuring point 4, and the impact stress amplitude at each point decreases in turn. It is consistent with the theoretical analysis; the reason is that the drill stem material has anelasticity [23], and the impact stress amplitude decreases with the increase of displacement.

In order to further clarify the attenuation law, the stress amplitude at each measuring point is then fitted according to equation (15), and the curve is obtained as shown in Figure 12. It can be seen that the stress attenuation trend in the drill stem basically satisfies the pure exponential attenuation equation. The stress at measuring point 4 was abruptly reduced due to the superposition effect of reflected stress, so this point was discarded in the curve fitting.

Secondly, in order to study the impact stress transfer characteristics in the drill stem under different impact input parameters, the variable impact energy and variable percussive frequency tests are carried out, respectively. The impact input parameters are shown in Table 3.

Figure 13(a) shows the variation trend of impact stress with single impact energy at different measuring points. It

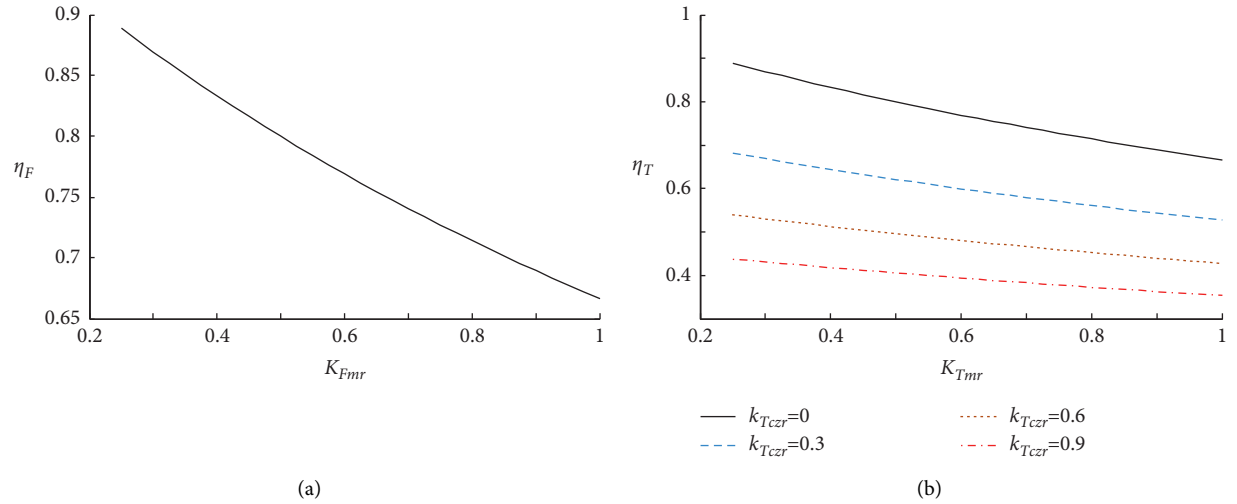

FIGURE 7: The drill flange/screw interface impact stress transmission efficiency. (a) Transmission efficiency of the flange interface. (b) Transmission efficiency of the screw interface.

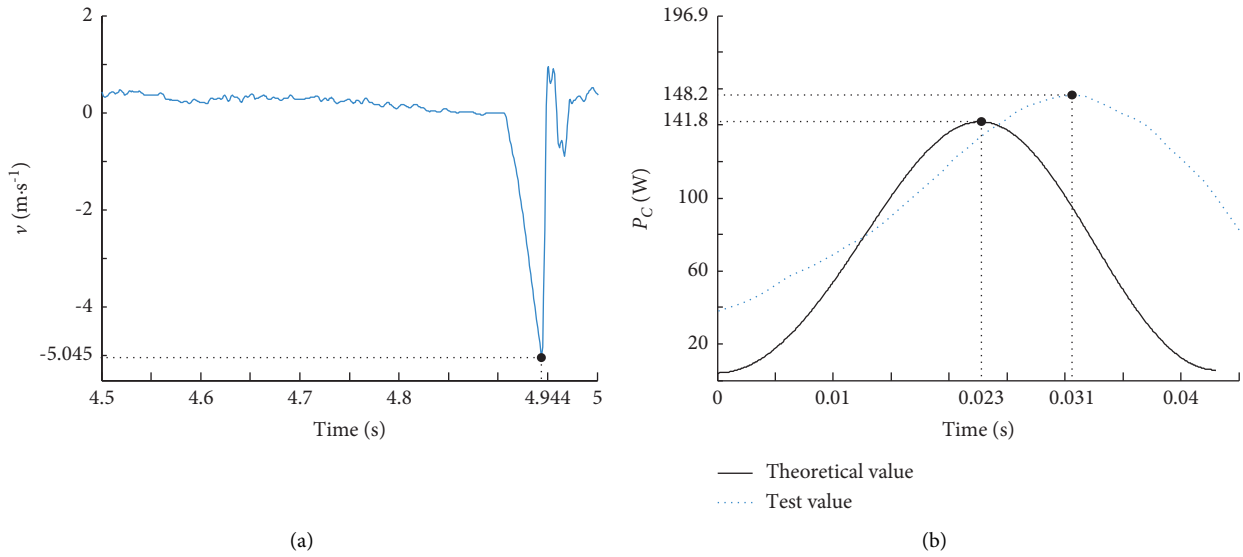

FIGURE 8: Curves of (a) velocity of the hammer and (b) percussive driving power.

can be seen that the impact stress amplitude at different measuring points on the drill stem increases with roughly a quadratic growth trend when single impact energy increases. It is consistent with the theoretical analysis which is that the impact energy will affect the magnitude of the input energy, and when the input energy is high, the impact stress is large.

Figure 13(b) shows the variation trend of impact stress with percussive frequency at different measuring points. It can be seen that the amplitude of impact stress at different measuring points on the drill stem increases with the increase of percussive frequency. This is because when the percussive frequency increases, the single impact energy of the percussive mechanism increases slightly. And as the frequency increases, the number of impact forces applied by the percussive mechanism per unit time also increases, which makes the impact stress interval transferred to the next measurement position decrease, thus increasing the probability of impact stress superposition.

3.3. Transfer Characteristics' Experiment at the Joints of Drilling Tools. In order to study the transfer characteristics of impact stress at the drilling tool joints, a fiber grating sensor can be installed at each of the drilling tool flange interface and screw interface. Figure 14 shows the variation trend of impact stress at the flange connection interface and screw connection interface, where the percussive frequency is 2 Hz and the static pressure is 100 N.

As can be seen from Figure 14, the impact stress does not change significantly past the drilling tool flange interface. This is mainly because at the drilling tool flange interface, the cross section of the anvil is larger than the cross section of

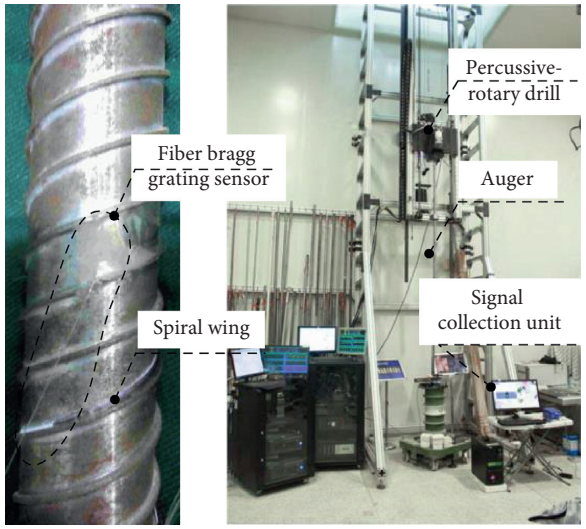

Figure 9: The drilling impact stress transfer characteristics' test system.

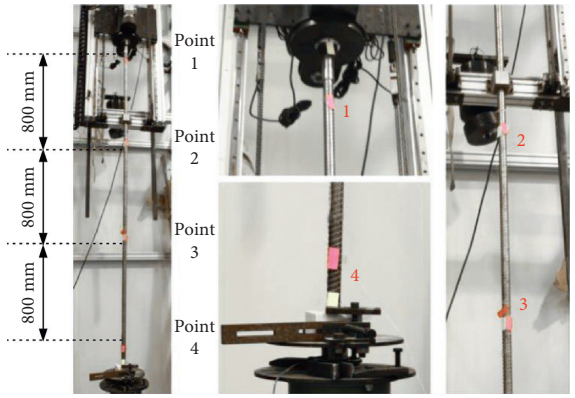

Figure 10: The layout of the fiber Bragg grating in the impact stress transmission test.

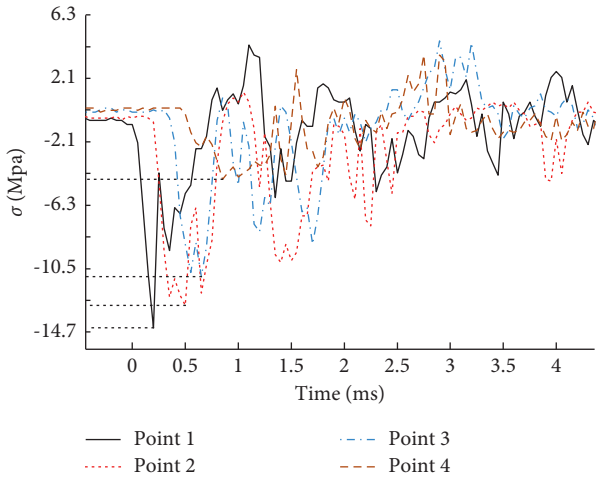

Figure 11: Curves of impact stress on drill different positions.

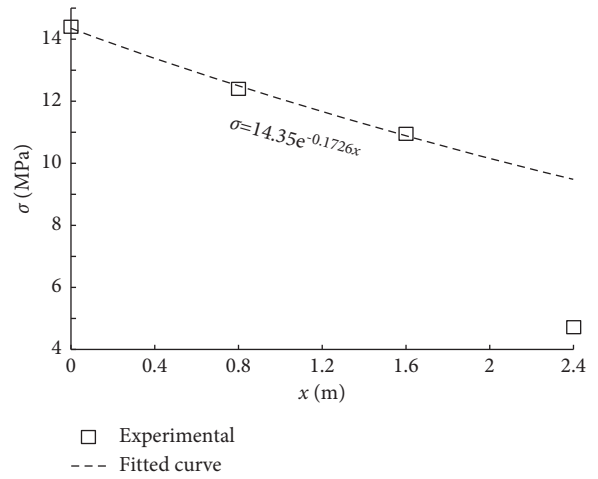

Figure 12: Impact stress attenuation curve in the drill stem.

Table 3: The input parameters of drilling tool impact stress.

Parameter name	Parameter range
F_p (Hz)	{2, 4, 6, 8, 10, 12, 14, 16}
W_P (J)	{1.3, 2.25, 3.125, 4}

the drill stem, and the impact stress is slightly amplified during the transfer from the large cross section to the small cross section, and this amplification effect will compensate for the lost impact stress. On the contrary, the impact stress loss is obvious when passing through the screw interface. Thus, in order to improve the transfer efficiency of impact stress, the screw connection length between the drill bit and the drill stem should be as short as possible when designing the drilling tool.

In order to make the theoretical model further predict the transfer efficiency at the drilling tool joints, the above test data need to be analyzed and calculated. After selecting the best equivalent mass ratio and equivalent damping ratio, the theoretical transfer efficiency can be obtained by substituting them into transfer models (17) and (18) and then compared with the measured transfer efficiency.

Figure 15 is the comparison of the theoretical and measured transfer efficiency. It can be seen that, under different impact energy conditions, the impact stress transfer efficiency at the flange interface and screw interface is basically consistent with the theoretical model. Therefore, the above transfer model can better predict the impact stress transfer efficiency at the drilling tool joints under different working conditions.

In addition, the impact stress may also be transmitted along the spiral direction on the drilling tool. Therefore, another fiber grating sensor can be placed at the same cross-sectional position of measuring point 3 to compare the difference between stress transmission characteristics along the axial and spiral directions on the drilling tool. Figure 16 shows the variation trend of impact stress at measuring point 3, in which the percussive frequency is 2 Hz and the static pressure is 100 N.

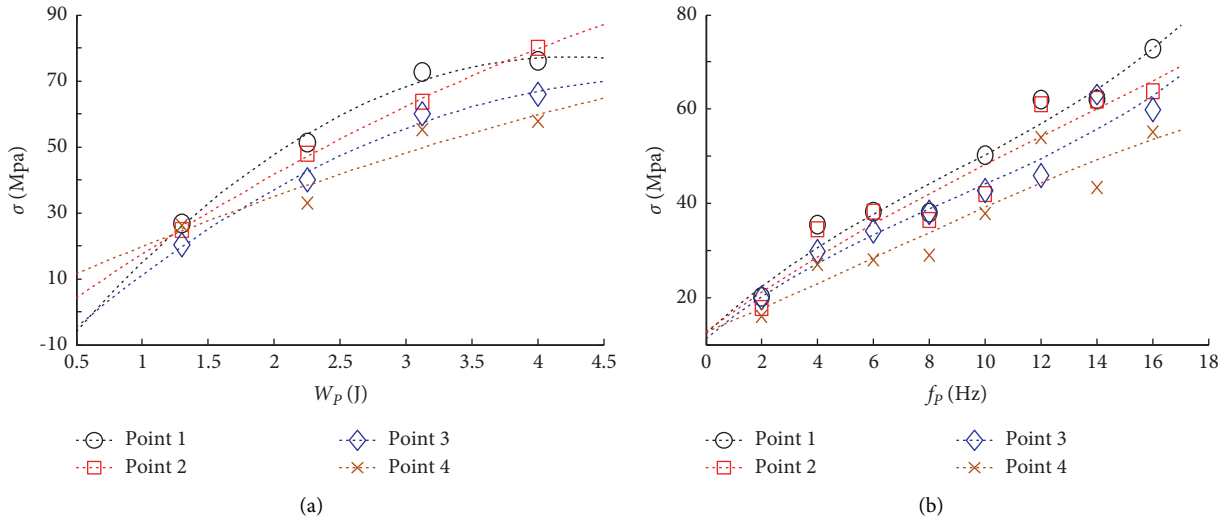

FIGURE 13: The impact stress at each measuring point under different input parameters. (a) Curves of impact stress vs. impact energy. (b) Curves of impact stress vs. percussive frequency.

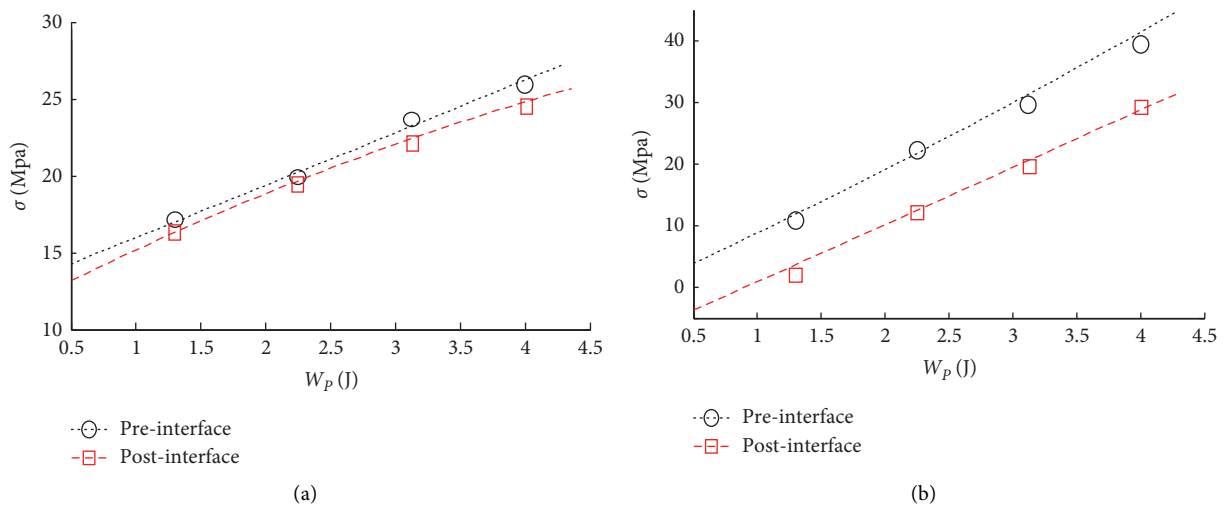

FIGURE 14: The impact stress transfer characteristics at the drilling tool joints. (a) The impact stress at the flange interface. (b) The impact stress at the screw interface.

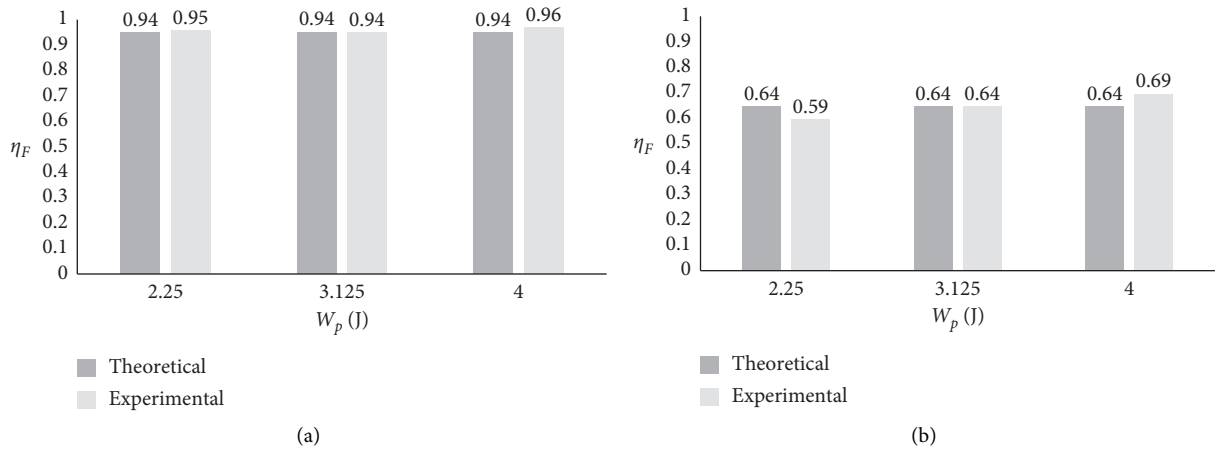

FIGURE 15: Comparison of the theoretical and measured transfer efficiency at drilling tool joints under different impact energies. (a) $K_{Fmr} = 0.13$, flange interface. (b) $K_{Tmr} = 0.42$ and $K_{Tczr} = 0.3$, screw interface.

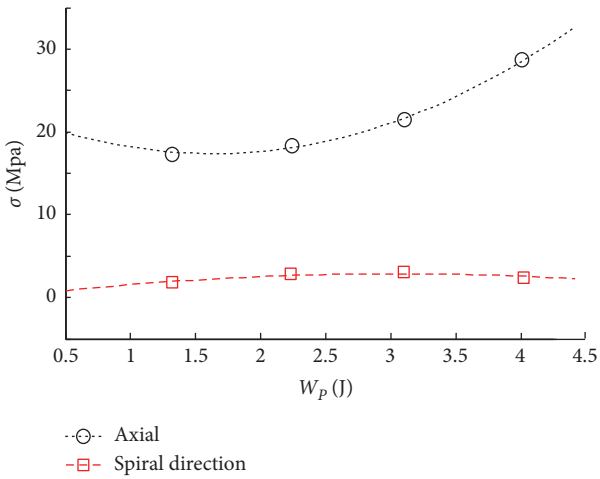

Figure 16: The impact stress transferred along the axial and spiral directions on the drilling tool.

As can be seen from Figure 16, there is also a certain impact stress along the spiral direction on the drilling tool, but it is much smaller than the impact stress transmitted along the axial direction of the drilling tool, and the change of impact energy has little effect on it. This indicates that the main transfer direction of impact stress in the drilling tool is axial, while the impact stress transferred along the spiral direction can be approximately neglected.

4. Conclusions

Aiming at how to improve the impact stress obtained at the cutting edge of the drill bit, this paper successively carried out the parameter optimization design of the percussive drive mechanism and the research on the transfer characteristics of the impact stress in the drilling tool. The transfer characteristics of the impact stress from generation, incidence to transfer to the cutting edge are clarified.

Eventually, it was found that increasing the percussive frequency and impact energy of the percussive mechanism as well as increasing the contact stiffness of the collision surface could improve the incident impact stress of the drilling tool. In addition, reducing the length of the screw connection between the drill bit and the drill stem can reduce the impact stress transfer loss, while the stress transfer loss at the drilling tool flange connection interface and in the spiral direction can be neglected. This provides a theoretical reference for the design of the percussive mechanism and drilling tools in lunar surface drilling and sampling tasks.

Data Availability

The data used to support the findings of this study are included within the article.

Conflicts of Interest

The authors declare that there are no conflicts of interest regarding the publication of this paper.

Acknowledgments

This work was financially supported by the National Science Foundation of China (51805008 and 52005136), the "Thirteenth Five-Year" Science and Technology Project of Jilin Provincial Department of Education (JJKH20200036KJ), and the Jilin Province Science and Technology Development Project (20200301044RQ).

References

[1] Z. Y. Ouyang, "Interpretation of the in-depth history of mankind's first lunar trip-the preface of apollo moon landing project," *Science Education and Museum*, vol. 5, no. 5, pp. 394-395, 2019.

[2] J. Liu, Z. Ouyang, and C. Li, "Progress in lunar exploration in China," *Bulletin of Mineralogy, Petrology and Geochemistry*, vol. 32, no. 5, pp. 544–551, 2013.

[3] P. G. Magnani, S. Senese, G. Cherubini, and A. Olivieri, "Different drill tool concepts," *Acta Astronautica*, vol. 59, no. 8-11, pp. 1014–1019, 2006.

[4] P. Ye, M. Yang, J. Huang, L. Meng, and Z. Sun, "The process and experience in the development of Chinese lunar probe," *Scientia Sinica Technologica*, vol. 44, no. 6, pp. 543–558, 2014.

[5] V. Badescu and K. Zacny, *Outer Solar System: Prospective Energy and Material resources*, Springer, Berlin, Germany, 2018.

[6] H. H. Cai and Z. B. Peng, "Exploring the drilling technology of extraterrestrial bodies with lunar drilling as an example," *Science & Technology Vision*, vol. 2015, no. 16, pp. 6-7, 2015.

[7] H. Z. Chem, S. Y. Jiang, and M. Zhang, "Design and research of astronaut hand-held high-frequency shock sampling device," *Journal of Deep Space Exploration*, vol. 2, no. 2, pp. 131–136, 2015.

[8] Q. Q. Quan, X. M. Shi, and D. W. Tang, "Extraction and identification of drilling features at the simulated lunar regolith-simulated lunar rock interface," *Robot*, vol. 37, no. 3, pp. 351–360, 2015.

[9] Z. Kris, P. Gale, and S. Mateusz, "Challenges and methods of drilling on the moon and mars," in *Proceedings of the 2011 Aerospace Conference*, pp. 1–9, IEEE, Big Sky, MT, USA, March 2011.

[10] L. Y. Li, "Research on the matching of impact performance and collision coefficient of hydraulic rock drill," *Shock and Vibration*, vol. 2021, Article ID 6651860, 13 pages, 2021.

[11] W. A. Hustrulid, "A bit-rock interaction model for rotary-percussive drilling," *International Journal of Rock Mechanics and Mining Sciences*, vol. 48, pp. 827–835, 2011.

[12] N. U. Mate, S. V. Bakre, and O. R. Jaiswal, "Comparative study of impact simulation models for linear elastic structures in seismic pounding," in *Proceedings of the 15 WCEE*, Lisboa, Portugal, September 2012.

[13] J. Wang, R. Luo, and Y. Hou, "Elasticmodel and experimental study of drill rod joint," *Pneumatic tools for rock drilling machinery*, vol. 4, pp. 23–26, 2014.

[14] F. Y. Li and S. J. Ma, "Analysis and experimental study of acceleration model for short interval and multiple impact equipment," *Shock and Vibration*, vol. 2019, Article ID 5139137, 15 pages, 2019.

[15] Y. Yang, H. Liao, Y. Xu, J. Niu, and L. Yang, "Theoretical investigation of the energy transfer efficiency under percussive drilling loads," *Arabian Journal of Geosciences*, vol. 12, no. 5, p. 175, 2019.

[16] W. Yuan, J. Chang, J. Jin et al., "The influence of axial static load on the amplitude of stress wave in variable cross-section rods," *Vibration and shock*, vol. 38, no. 17, pp. 51–57+72, 2019.

[17] Q. Q. Quan, P. Li, S. Y. Jiang et al., "Development of arotary percussive drilling mechanism," in *Proceedings of the 2012 IEEE International Conferenceon Robotics and Biomimetics*, Guanzhou, China, December 2012.

[18] D. Jie, P. Li, Q. Quan et al., "Optimization of percussive mechanism in rotary-percussive drill for lunar exploration," in *Proceedings of the 2013 IEEE International Conference on Robotics and Biomimetics*, Shenzhen, China, December 2013.

[19] P. Li, H. Zhang, S. Y. Jiang, and W. Zhang, "Analysis and testing of load characteristics for rotary-percussive drilling of lunar rock simulant with a lunar regolith coring bit," *Shock and Vibration*, vol. 2017, Article ID 3012749, 15 pages, 2017.

[20] A. Ivan and J. Marko, "Longitudinal elastic stress impulse induced by impact through a spring-dashpot syst-em:Optimization and inverse problems for the spring stiffness," *International Journal of Solids and Structures*, vol. 50, pp. 3960–3966, 2013.

[21] Z. L. Chen, "Research on impact stress transfer and crushed rock load characteristics of deep core drilling tools," Master's Degree thesis, Harbin Institute of Technology, Harbin, China, 2016.

[22] S. H. Sun, Y. L. Yu, and H. Li, "Research on stress wave detection technology based on fiber grating," *China Laser*, vol. 43, no. 5, pp. 505002–505011, 2016.

[23] H. T. Zhang, L. J. Ma, Z. M. Luo, and N. Zhang, "Wave attenuation and dispersion in a 6 mm diameter viscoelastic split hopkinson pressure bar and its correction method," *Shock and Vibration*, vol. 2020, Article ID 8888445, 10 pages, 2020.